Solidification and Age Hardening Behaviour of Mg-Zn-Gd Alloys

2012 IOP Conf. Ser.: Mater. Sci. Eng. 27 012021

(http://iopscience.iop.org/1757-899X/27/1/012021)

Solidification and Age Hardening Behaviour of Mg-Zn-Gd Alloys

J H Li [1] and P Schumacher [1, 2]
[1] Chair of Casting Research, the University of Leoben, Leoben, Austria
[2] Austrian Foundry Research Institute, Leoben, Austria

E-mail: jie-hua.li@hotmail.com

Abstract. The solidification and age hardening behaviour of an Mg-6Zn-2Gd (wt. %) alloy has been investigated. It was found that the microstructure of the as-cast samples was composed of equiaxed α-Mg grains surrounded by some eutectic compound both at triple points and along grain boundary. The eutectic compound was composed of $MgZn_2$, Mg_5Gd phases and α-Mg matrix. After a solution treatment at 500 °C for 18 h, the eutectic compound almost dissolved, but some discontinuous second phase particles still survived at grain boundaries. The $Mg_3Gd_2Zn_3$ phase also formed during subsequent ageing. The addition of Gd not only improved the thermal stability of the second phase formed during solidification, but also postponed the overaging during ageing at 200 °C up to 100 h. The precipitates with three different morphologies: $[0001]_\alpha$ rods/lath, $(0001)_\alpha$ plates and blocky particles, were observed in the α-Mg matrix. The solute elements of Zn and Gd were found to significantly partition into the precipitates, especially for blocky particles. This significant partition can be correlated directly to improved mechanical properties at elevated temperature.

1. Introduction

Magnesium alloys have great potential for the application in automotive and aerospace application due to their high specific strength [1]. The Mg-Zn based alloys, i.e. ZK51 (Mg-4.5Zn-0.6Zr (wt. %)), have been widely used as a wrought Mg alloy. However, these wrought Mg-Zn based alloys are susceptible to micro-porosity and are not weldable. There is a need for research on the solidification behaviour during casting of Mg-Zn based alloys. Furthermore, the precipitates formed in binary Mg-Zn alloys during artificial ageing are generally coarse and inhomogeneously distributed [2]. The high temperature mechanical properties of Mg-Zn binary alloys, especially the creep-resistant properties, become inadequate for technological applications at a temperature above 250 °C. Research on the age hardening behaviour of Mg-Zn based alloy is of great importance to further improve the age hardening response by controlling the decomposition of the supersaturated solid solution of zinc in magnesium [3].

Some alloying elements, i.e. Cr [4], Cu [5, 6], Ti [7], Ba [8], Ag [9], Ca [10, 11], RE (Y [12], Gd [13, 14]) et al, were added into Mg-Zn binary alloys, with the aim to improve the age hardening effect. Among these elements, Gd has often been used since the solid solubility of Gd in Mg at 548 °C is as high as 4.53 at. % (23.49 wt. %), and decreases to 0.61 at. % (3.82 wt. %) at 200 °C [3]. The Mg-Zn-

Gd system is thought to be promising to develop high strength Mg alloys since precipitates can be formed on the basal plane [15, 16, 17] or both on the prismatic and basal plane [18].

Especially, an Mg-6Zn-2Gd (wt. %, short for ZG62) alloy has been reported to have increased mechanical properties [13, 14]. Above 200°C, the TYS and UTS of ZG62 alloy is slightly higher than that of a Gd-free alloy. More importantly, the elongation of the ZG62 alloy at 300 °C (40.5 %) is much higher than that of Gd-free alloy (10 %), which is very attractive for the application of Mg alloy at higher temperature. However, the solidification behaviour and the precipitates formed in this alloy have not been well understood. Especially, there is a lack of understanding on the solute partitioning during the formation of precipitates. In this paper, we focus on the Mg-6Zn-2Gd-0.6Zr (wt. %) alloy to characterize solidification microstructures and precipitates in detail. These detailed structural and chemical composition investigation are aimed to elucidate the solidification and age hardening behaviour.

2. Experimental methods

The Mg-6Zn-2Gd-0.6Zr alloy (wt. %, used throughout the paper, in case not specified otherwise) was prepared from pure Mg (99.9%), Zn (99.9%), Mg–28Gd and Mg–33Zr master alloys in an electric resistance furnace under an anti-oxidizing flux as protection, and then cast into a sand mould. Solution treatment was performed in a salt bath at 500 °C for 18 h, followed by quenching into cold water and then ageing in oil at 200 °C for up to 100 h.

Differential scanning calorimetry (DSC) (Q600SDT) was conducted under the protection of pure Ar at a heating rate of 10 °C/min. X-ray diffraction patterns were collected using a Cu target. The X-ray data collection was performed in the range from 20 ° to 80 °. A slow scanning speed (0.2 °/min) was used. A heating stage for in-situ temperature scans up to 300 ° was employed to heat samples. Before each test, samples were given a holding time of 5 min to equilibrate the temperature. Vickers hardness testing was performed using a LECO Hardness Tester (LV700AT) with 50 N load and 15 sec dwell time. Each data point reported in this paper represents an average of at least 10 measurements.

Optical microscopy (OM) characterization was performed using Zeiss Axioskop 2 MAT light microscopy. Scanning electron microscopy (SEM) was conducted using Zeiss ULTRA plus. The TEM specimens were prepared by electro-polishing in a solution of 25 % $HClO_4$ and 75 % methanol at about – 40 °C and 18 V. Transmission electron microscopy (TEM) characterizations were performed using CM12 operating at 120 kV. Tips for APT analysis were prepared by standard two-step electropolishing from rods of approximately 0.5x0.5x15 mm. The first step used an electrolyte of 25 % percholoric acid in acetic acid at 15 V. The second step used an electrolyte of 2 % percholoric acid in 2-butoxethynal at 15 V. Reconstruction parameters were deduced using an approach outlined by Gault et al. [19]. Atom probe tomography (APT) characterizations were performed using an Imago LEAP™ 3000 at a specimen temperature of 20 K, 20 % pulse fraction and under ultrahigh vacuum conditions. Scheil simulation using Thermo-calc software with TTMg4 database was also performed to predict the phases present in the alloys and their formation temperatures.

3. Results and discussion

3.1. Microstructures of as-cast ZG62 alloy and after a solution treatment

Figure 1 shows microstructures of the ZG62 alloy both in the as-cast condition and after a solution treatment. The microstructure of the as-cast sample was composed of equiaxed α-Mg grains surrounded by eutectic at triple junctions and grain boundaries, as shown in figures. 1a, c. The mean grain size of the ZG62 alloy was measured to be approximately 35 μm using a linear intercept method. This grain size is similar to that observed in a ZK60 alloy with 1.3% Gd addition, but significantly less than that of ZK60 alloy (71 μm) [14]. This result is consistent with other observations that the addition of Gd (less than 2 wt. %) refines the microstructure [13, 14]. After solution treatment at 500 °C for 18 h, the eutectic structures in ZG62 alloy almost dissolve but some discontinuous second phase particles

survive on the grain boundary, as shown in figures 1b, d. Energy dispersive X-ray (EDX) spectra of particles, as marked with white arrows shown in figure 1 d, indicated the particles were enriched with Zn (about 17 wt. %, 9 at. %) and Gd (about 20 wt. %, 4 at. %), as shown in Figure 1e.

XRD patterns of the as-cast sample, as shown in figure 2, indicated that the microstructure consisted of α-Mg matrix and eutectic phase (α + Mg_5Gd + $MgZn_2$). This is fully consistent with the thermodynamic calculation of Mg-6Zn based alloys with an addition of Gd (1, 2, 3 wt. %), as shown in figure 3. The solidification path of these Mg-Zn-Gd alloys follows: L→ α-Mg + Mg_5Gd + $MgZn_2$. While the eutectic reaction temperature increases from 360 °C to 435 °C with increasing Gd content from 1 wt. % to 3 wt. %. After a T6 treatment (solution treatment at 500 °C for 18 h and subsequent aged treatment at 200 °C for 15 h), the Mg3Gd2Zn3 phase formed. The Mg3Gd2Zn3 phase was believed to form via the diffusion of Zn and Gd in the α-Mg matrix. This phase was not predicted in Scheil simulation using Thermo-calc software. Equilibrate Dictra simulation considering the diffusion during ageing is required. XRD results revealed that the Mg3Gd2Zn3 phase shows a better thermal stability at higher temperature, as shown in figure 2 (line 3, 4, 5). In contrast, the peaks of Mg5Gd and MgZn2 phases became weaker.

After a solution treatment at 500 °C for 18 h and subsequent ageing at 200 °C for 15 h, some finer precipitates also observed in the α-Mg matrix. These finer precipitates formed in the α-Mg matrix are described in next Section 3.3.

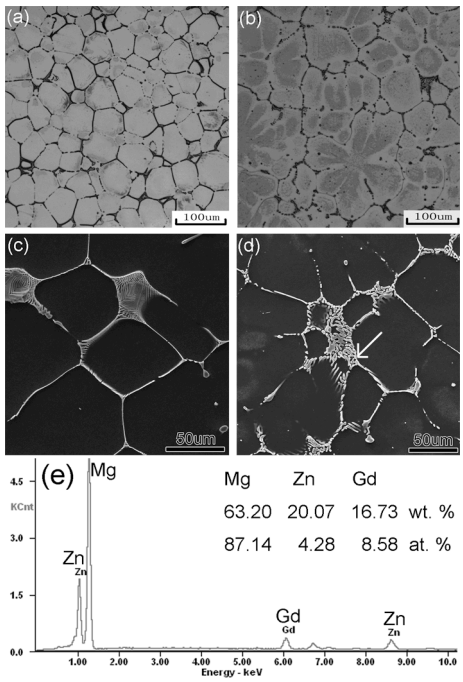

Figure 1. Microstructure of Mg-6Zn-2Gd-0.6Zr (wt. %) alloy. (a), (b), optical microscopy image; (c), (d), SEM image. (a), (c) as-cast; (b), (d) after a solution treatment at 500 °C for 18 h; (e) the energy dispersive X-ray (EDX) spectra analysis results of the particles, as marked in figure 1 d.

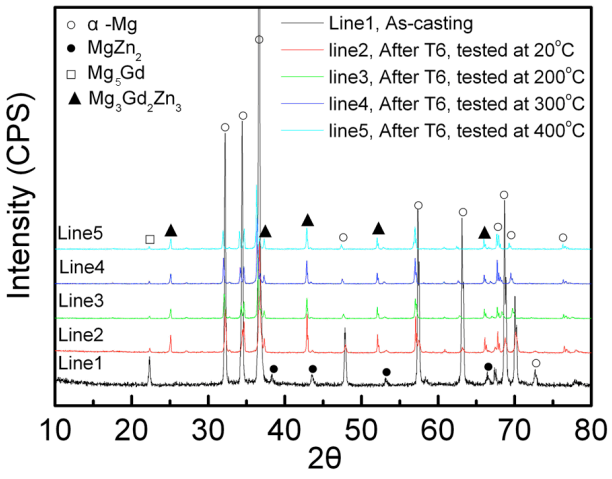

Figure 2. XRD results of the Mg-6Zn-2Gd-0.6Zr (wt. %) alloy. The $MgZn_2$ and Mg_5Gd phase (line 1) formed during solidification. The $Mg_3Gd_2Zn_3$ phase (lines 2-5) formed after a T6 treatment.

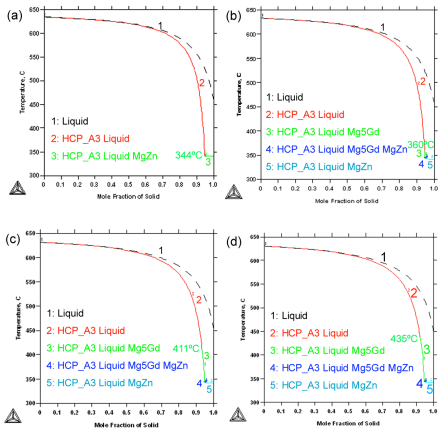

Figure 3. Calculated phase fraction vs. temperature for Mg-6.0 Zn alloys containing (a) 0 wt. % Gd, (b) 1.0 wt. % Gd, (c) 2.0 wt. % Gd, (d) 3.0 wt. % Gd according to Scheil´s model.

3.2. Age hardening response of the ZG62 alloy

Figure 4 shows the age hardening response of the ZG62 alloy at 200 °C. The hardness did not change significantly at the beginning of the ageing treatment up to 50 h. With increasing ageing time, the hardness increased greatly, and reached its peak hardness (72 HV) at about 80 h. A further increase in ageing time resulted in a gradual decrease in hardness. Such phenomenon was also observed in an Mg-4.5Zn-2Gd (wt. %) alloy [13]. The peak hardness of the ZG62 alloy was equivalent to that of Mg-8Zn-1.5MM (MM, a mixture of approximately 50Ce, 25La, 20Nd, and 3Pr) and Mg-4Zn-1.5MM, but considerably greater than that of binary Mg-9Zn alloy according to hardness values reported in literature [20]. Moreover, the peak hardness occurred after about 80 h ageing for ZG62 alloy, much later than 10 h for Mg-9Zn alloy and 20 h for Mg-8Zn-1.5RE and Mg-4Zn-1.5RE. This indicates that the addition of Gd into Mg-Zn alloy postpones the age-hardening response of the alloy.

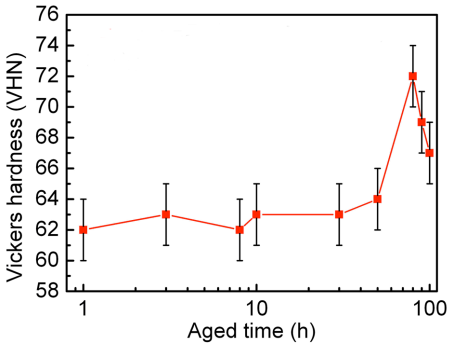

Figure 4. Age hardening response of Mg-6Zn-2Gd-0.6Zr (wt. %) alloy aged at 200 °C up to 100 h.

3.3. Precipitates in the ZG62 alloy

Figure 5 shows the $[01\bar{1}1]_\alpha$, $[1\bar{2}1\bar{3}]_\alpha$, $[01\bar{1}0]_\alpha$ bright field TEM images (a), (c), (e) and corresponding SADPs (b), (d), (f) of the precipitates obtained from the ZG62 alloy aged at 200 °C for 15 h. Viewed from three different direction, it is clear that the precipitates with three different morphologies, i.e. $[0001]_\alpha$ rods/lath, $(0001)_\alpha$ plates and blocky particles, as marked with white arrows and labeled as 1, 2 and 3 in figure 7a, are present in the α-Mg matrix. This is consistent with the observation in an Mg-Zn alloy [20, 21]. The $[0001]_\alpha$ rods (labeled as 1) have been commonly regarded as β'_1, while the $(0001)_\alpha$ plates (labeled as 2) were commonly taken as β'_2 in previous studies [3, 20-23]. Both β'_1 and β'_2 have a hexagonal structure (a=0.523nm, c=0.858nm) [20, 23] which is identical to that of Laves phase $MgZn_2$ [23].

After ageing at 200 °C for 80 h, the number density of the $[0001]_\alpha$ lath with a larger aspect ratio on the cross section (marked with the white arrow and labeled as 1 in Figure 6a), are still dominant, although a mixture of $[0001]_\alpha$ rods/lath, $(0001)_\alpha$ plates and blocky particles are present in the microstructure. This is in contrast to the reports in a Mg-Zn alloy [20, 21] and Mg-Zn-RE alloy [20], where $[0001]_\alpha$ rods (β'_1) were reported to transform into $(0001)_\alpha$ plates (β'_2), and the β'_2 precipitates became dominant in the microstructure with increasing ageing time. It is generally believed that the formation of a fine dispersion of rodlike β'_1 precipitates play an important role during age hardening, while extensive precipitation of disc-shaped β'_2 precipitates coincides with the onset of overageing [20]. In this study, the dominant distribution of the β'_1 precipitates after ageing for 80 h indicates that the addition of Gd can retard the overaging in the present ZG62 alloy. This may account for why the peak hardness of the alloy was achieved at 80 h (Figure 4).

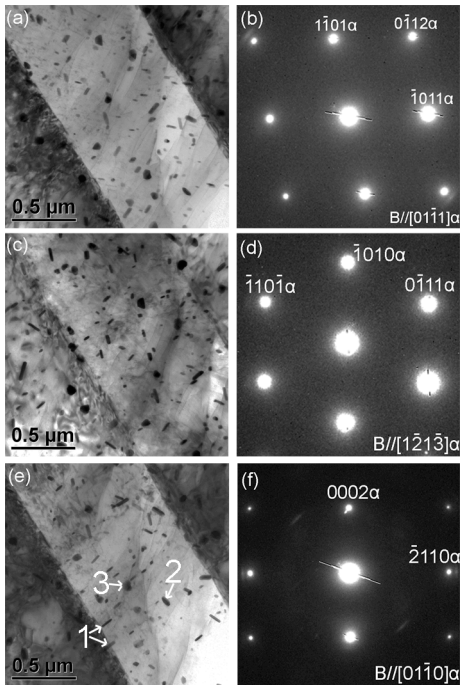

Figure 5. Bright field TEM images (a), (c), (e) and corresponding $[01\bar{1}1]_\alpha$, $[1\bar{2}1\bar{3}]_\alpha$, $[01\bar{1}0]_\alpha$ SADPs (b), (d), (f) of the precipitates obtained from Mg-6Zn-2Gd-0.6Zr (wt. %) alloy aged at 200 °C for 15 h.

3.4. APT characterisation of the precipitates in the ZG62 alloy

Figure 7 provides a representative three-dimensional atom maps recorded from atom probe experiments on specimens of the ZG62 alloy after ageing at 200 °C for 15 h. It was evident that all the alloying elements (Mg, Zn and Gd) were detected, as shown in Figure 7a. The main solute elements of Zn and Gd partitioned into the precipitates, as shown in figures 7b, c. By examining the precipitates from different directions, it was clear that most precipitates (marked as 1 in figure 5e) were elongated with their longitudinal axis parallel to $[0001]_\alpha$. This is in agreement with previous TEM observations of $[0001]_\alpha$ rods/ lath. In addition, some blocky particles (marked as 3 in figure 5e) have also been detected in atom probe experiments.

A selection box type method was used to measure the precipitate composition [24]. The composition measured across the precipitate was plotted in figures 7d, e. The blocky particle contains 60 at. % Zn and 5 at. % Gd, while the $[0001]_\alpha$ rods/ lath contains 6 at. % Zn and 1.5 at. % Gd. This indicates again that the solute elements of Zn and Gd partition significantly into the precipitates, especially for the blocky particles. This significant partition can be correlated directly to the observed thermal stability and the higher mechanical properties at elevated temperature, as reported elsewhere [25].

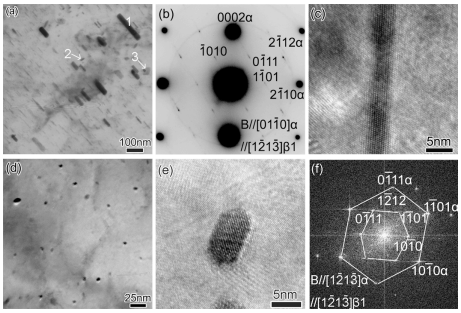

Figure 6. $[01\bar{1}0]_\alpha$ bright field TEM image (a), corresponding SADP (b) and HRTEM (c); $[\bar{1}2\bar{1}3]_\alpha$ bright field TEM image (d), HRTEM (e) and corresponding fast Fourier transformation (f) of Mg-6Zn-2Gd-0.6Zr (wt. %) alloy samples aged at 200 °C for 80 h.

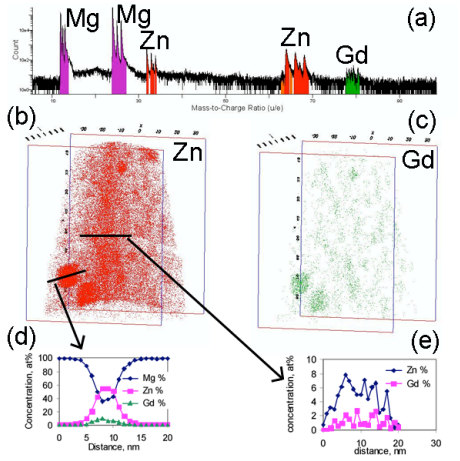

Figure 7. Typical mass spectrum under laser pulsing (a), atom probe elemental maps ((b) Zn (red), (c) Gd (green)) and solute concentrations across the precipitates ((d) blocky, (e) $[0001]_\alpha$ rods/lath) of Mg-6Zn-2Gd-0.6Zr (wt. %) alloys aged at 200 °C for 15 h.

4. Summary

The as-cast microstructure of ZG62 alloy consisted of α-Mg matrix and a eutectic phase (α+Mg_5Gd+$MgZn_2$). The $Mg_3Gd_2Zn_3$ phase also formed during the subsequent heat treatment. The addition of Gd not only improved the thermal stability of the second phase formed during solidification, but also postponed the overaging during ageing at 200 °C up to 100 h. This paper highlights the importance in improving the thermal stability of the second phase and the precipitates in order to produce high strength Mg alloy.

Acknowledgments

J.H. Li is grateful for scientific and technical input and support from the Australian Microscopy & Microanalysis Research Facility (AMMRF) node at the University of Sydney. J.H. Li also gratefully acknowledges Prof. G. Dehm for the access to the TEM facilities at the Erich Schmid Institute of Materials Science of the Austrian Academy of Science, Leoben.

References

[1] Smola B, Stulíková I, von Buch F and Mordike B L 2002 *Mater. Sci. Eng. A* **A324** 113-117.
[2] Clark J B *Acta Metall.* 1965 **13** 1281-1289.
[3] Clark J B, Zabdyr L and Moser Z, 1988 *Phase Diagram of Binary Magnesium Alloys*, Nayeb-Hashemi A A, Clark J B (Eds.), (Metals Park, OH; ASM International) 353-355.
[4] Buha J 2008 *Mater. Sci. Eng. A* **A492** 293-299.
[5] Lorimer G W *Magnesium Technology* 1986 (London:Institute of Metals) 47-53.

[6] Unsworth W and King JF *Magnesium Technology*, Institute of Metals, London, 1987, pp. 25-31.
[7] Buha J 2008 *J. Mater. Sci.* **43** 1220-1227.
[8] Buha J 2008 *Mater. Sci. Eng. A* **A491** 70-79.
[9] Mendis C L, Oh-ishi K and Hono K 2007 *Scripta Mater.* **57** 485-488.
[10] Bettles C J, Gibson M A and Venkatesan K 2003 *Scripta Mater.* **51** 193-198.
[11] Oh J C, Ohkubo T, Mukai T and Hono K 2005 *Scripta Mater.* **53** 675-679.
[12] Zhou H T, Zhang Z D, Liu C M and Wang Q W 2007 *Mater. Sci. Eng. A* **A445-446** 1-6.
[13] Yang J, Wang LD, Wang L M and Zhang H J 2008 *J. Alloys Compd.* **459** 274-280.
[14] He S M, Peng L M, Zeng X Q, Ding W J and Y.P. Zhu Y P 2006 *Mater. Sci. Eng. A* **A433** 175-181.
[15] Nie J F, Gao X and Zhu S M 2005 *Scripta Mater.* **53** 1049-1053.
[16] Gao X and Nie J F 2008 *Scripta Mater.* **58** 619-622.
[17] Nie J F, Oh-ishi K, Gao X and Hono K, *Acta Mater.* **56** 6061-6076.
[18] Sha G, Li J H, Wang T Y, Jie WQ and Ringer S P *Mater. Sci. Eng. A* (To be published).
[19] Moody M P, Gault B, Stephenson L T, Haniel D and Ringer S P (2009) *Ultramicroscopy*, *109* 815-824.
[20] Wei L Y, Dunlop G L and Westengen H 1995 *Metall. Mater. Trans. A* **26A** 1705.
[21] Gao X and Nie J F 2007 *Scripta Mater.* 56 645-648.
[22] Rokhlin L L and Oreshkina,A A 1988 *Fiz. Metal. Metalloved.* **66** 559.
[23] Komura Y and Tokunaga K 1980 *Acta Crystallogr.* **36B** 1548.
[24] Vaumousse D, Cerezo A and Warren P J 2003 *Ultramicroscopy* **95** 215.
[25] Yang G Y, Li J H, Jie, W Q and Yu Z 2010 Mater. Sci. Forum **654-656** 651-654.